LANGMUIR

pubs.acs.org/Langmuir Article

Water Wettability Coupled with Film Growth on Realistic Cyclopentane Hydrate Surfaces

Hannah M. Stoner, Anh Phan, Alberto Striolo, and Carolyn A. Koh*

Cite This: *Langmuir* 2021, 37, 12447−12456 Read Online

ACCESS | Metrics & More | Article Recommendations | Supporting Information

ABSTRACT: Although the wettability of hydrate surfaces and hydrate film growth are key to understanding hydrate agglomeration and pipeline plugging, a quantitative understanding of the coupled behavior between both phenomena is lacking. *In situ* measurements of wettability coupled with film growth were performed for cyclopentane hydrate surfaces in cyclopentane at atmospheric pressure and temperatures between 1.5−6.8 °C. Results were obtained as a function of annealing (conversion) time and subcooling. Hydrate surface wettability decreased as annealing time increased, while hydrate film growth rate was unaffected by annealing time at any subcooling. The results are interpreted as a manifestation of the hydrate surface porosity, which depends on annealing time and controls water spreading on the hydrate surface. The wettability generally decreased as the subcooling increased because higher subcooling yields rougher hydrate surfaces, making it harder for water to spread. However, this effect is balanced by hydrate growth rates, which increase with subcooling. Also affecting the results, surface heating from heat release (from exothermic crystallization) allows excess surface water to promote spreading. The hydrate film growth rate on water droplets increased with subcooling, as expected from a higher driving force. At any subcooling, the instantaneous hydrate growth rate decreased over time, likely from heat transfer limitations. A new phenomenon was observed, where the angle at the three-phase point increases from the initial contact angle upon hydrate film growth, named the crystallization angle. This is attributed to the water droplet trying to spread while the thin film is weak enough to be redirected. Once the hydrate film grows and forms a "wall" around the droplet, it cannot be moved, and further growth yields a crater on the droplet surface, attributed to water penetrating the hydrate surface pore structures. This fundamental behavior has many flow assurance implications since it affects the interactions between the agglomerating hydrate particles and water droplets.

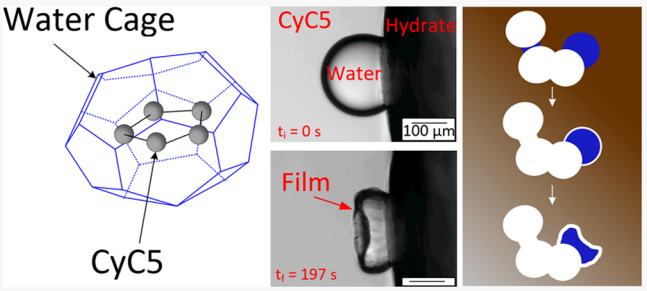

INTRODUCTION

Clathrate hydrates (i.e., hydrates) are crystalline inclusion compounds composed of a cage structure of hydrogen-bonded water molecules enclosing different kinds of guest molecules. Hydrates form under specific pressure and temperature conditions, making them a common occurrence naturally in both marine and permafrost deposits[1] and in subsea or arctic petroleum flowlines.[2] They also have many scientific and technical applications, including gas transportation/storage,[3] water desalination,[4,5] and gas separation.[6,7] Hydrate unit cells are comprised of a few different cages, including the 5^{12}, $5^{12}6^2$, and $5^{12}6^4$ cages, which are the most common. Here, the base number indicates the shape of the face (5 is a pentagon, 6 is a hexagon), and the exponent indicates how many of each face are present in the cage (i.e., the 5^{12} cage has 12 pentagonal faces). These cages come together to form the two most common hydrate crystal structures, known as structure I (sI) and structure II (sII). Generally, natural hydrate deposits are sI and contain only small molecules, like methane, to fill each cage. Flowline hydrates are generally sII, as the larger hydrocarbons (ethane, propane, etc.) can stabilize the larger $5^{12}6^4$ cage.[8]

As it can be difficult to study natural gas hydrates due to the high-pressure requirement, some low-pressure analogues have been used to study interfacial behavior, including tetrahydrofuran (THF) and cyclopentane (CyC5) hydrates. Extensive work has been done using THF hydrates,[9−11] but Taylor et al.[12] and Dieker et al.[13] raised concerns about ice contamination; because the equilibrium conditions for atmospheric THF hydrate formation is ∼4.4 °C, to facilitate hydrate formation, sufficient subcoolings are often applied that bring the temperatures below the ice point, thus making it difficult to confirm whether solid structures are ice or hydrate. Because Dieker[14] showed that CyC5 forms sII hydrates that are stable at atmospheric pressure and temperatures up to 7.7 °C above the ice melting temperature, the present study uses

Received: August 10, 2021
Revised: September 24, 2021
Published: October 13, 2021

https://doi.org/10.1021/acs.langmuir.1c02136
Langmuir 2021, 37, 12447−12456

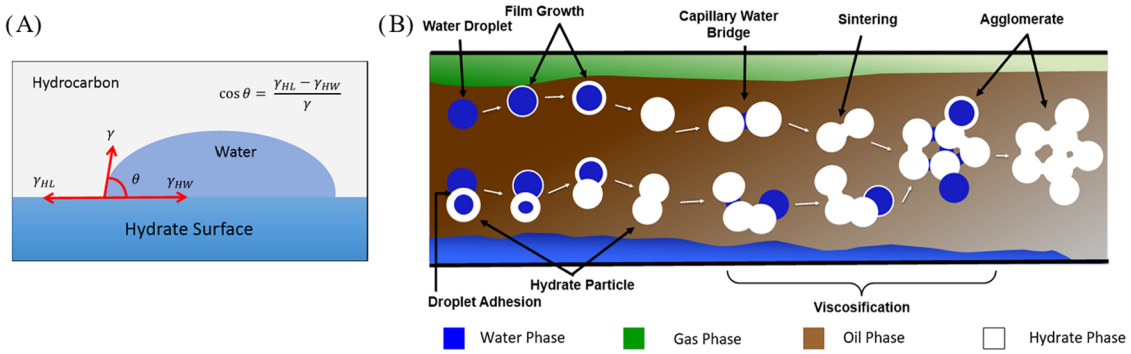

Figure 1. (A) Visualization of the contact angle on an ideal surface in terms of a hydrate surface (H)/water (W)/liquid hydrocarbon (L) system. The terms in the Young equation are the contact angle of the three-phase line (θ), the surface tension between the hydrate surface and the liquid hydrocarbon (γ_{HL}), the surface tension between the hydrate surface and the water (γ_{HW}), and the interfacial tension between the water and the liquid hydrocarbon (γ). (B) Hydrate agglomeration in a multiphase flowing pipeline. Initial hydrate growth on a water droplet is controlled by wettability and film growth, which leads to sintering and viscosification through droplet adhesion or capillary bridging. Extensive hydrate growth and agglomeration can lead to jamming and plugging of a flowline.[20] The top path represents water droplets directly converting to hydrate through film growth, and the bottom path represents contact-induced agglomeration.[21]

CyC5 hydrates as a model analogue for the flowline sII hydrates. In our experiments, the temperature is raised above the ice melting temperature to destabilize ice while preserving CyC5 hydrates.

Interfaces are particularly important for hydrates, as their formation occurs at the water−hydrocarbon interface and because wettability is often related to the extent of film growth and agglomeration tendency in a given system. Formation at the interface occurs because of differences in solubility, where the mole fraction of gases in hydrates is generally much larger than the solubility of those gases in water. For example, X_{CH4} in water = 0.000839 ≪ X_{CH4} in hydrate = 0.15.[15] It is also worth pointing out that X_{H2O} in CH_4 = 0.001 ≪ X_{H2O} in hydrate = 0.85.[16] This also applies to CyC5 hydrates.[17] Wettability is frequently quantified through contact angle measurements, with higher wettability indicating that a water droplet will spread over a larger area on the hydrate surface, promoting agglomeration through capillary bridging, whereas a lower wettability indicates low water spreading. High wettability results in small contact angles, and low wettability results in large contact angles. The contact angle (θ) can be calculated using the Young equation, which relates the contact angle to different interfacial tensions.[18] This equation is only applicable for ideal surfaces, of which hydrates in realistic conditions are not.[19] The contact angle can also be directly measured *in situ* as the angle made between the solid hydrate surface and the water−hydrocarbon interface, as shown in Figure 1A. Identifying the contact angle and wettability behavior at the interfacial level is essential in understanding the hydrate formation process.

Despite the difficulties, recent progress has been made in the measurement of contact angles for hydrate systems,[22−25] particularly for CyC5 hydrates. In 2018, Brown et al.[26] reported the average, finite contact angle of water on a CyC5 hydrate in liquid CyC5 as 94.2 ± 8.5° at atmospheric pressure and temperatures between 0 and 7.7 °C. In those experiments, 30 min of annealing time was applied.[26] Here, annealing time is defined as the total time elapsed between the beginning of the experiment, where the specified temperature is reached and the time when the measurements are taken. During this time, the unconverted water in the hydrate system is allowed to convert to hydrate undisturbed. It is not known how long the annealing time should be to allow all of the water to convert to hydrate. It has been previously shown through Raman spectroscopy[27] that the hydrate surface is porous; these pores become smaller over time as water on the hydrate surface and in the pores converts to hydrate. Pore reduction can limit the ability of the surface pores to draw water in through capillary action, which ultimately decreases the wettability and, therefore, increases the contact angle of a water droplet. It appears that the preparation of the hydrate surface can strongly affect contact angle measurements. In 2021, Thomas et al. reported dynamic spreading behavior and a fully wetted hydrate after 7 s of contact between a water droplet and the CyC5 hydrate surface.[28] As opposed to Brown et al.,[26] who used an annealing time of 30 min, Thomas et al.[28] used temperature cycling to form the hydrate over a period of ∼24 h, similar to the techniques used by Zylyftari et al.[29] Also, it has been shown that the driving forces (i.e., pressure and subcooling) affect hydrate surface roughness, which directly affects wetting.[30] Subcooling is often referred to as an indicator of driving force for hydrate growth,[8] but it should be noted that high subcoolings that lead to fast initial crystal growth can lead to heat transfer limitations due to their need to dissipate heat from the crystal surface.[8] Servio and Englezos have shown using methane and CO_2 hydrates that lower driving forces result in a smoother hydrate surface, whereas higher driving forces give a rougher surface and dendritic growth due to heat transfer limitations.[31] Hydrate roughness has also been measured for CO_2 hydrates at the CO_2−water interface using X-ray diffraction and reflectivity by Lehmkühler et al.[32] Both hydrate porosity and surface roughness play a role in the spreading of the water droplets on the hydrate surface, explaining the different results reported in the literature.[26,28] A relationship between subcooling and surface morphology/roughness has been suggested for CH_4/C_2H_6 hydrates.[33] Understanding the discrepancies between the reported contact angle values is essential for this field, as the contact angle can greatly affect the estimated hydrate−water interfacial interactions and cohesive/adhesive force values when modeling hydrate systems and their tendency for particle agglomeration and plugging risk.

Hydrate film growth is also an important interfacial phenomenon because it relates how quickly hydrate conversion occurs in practical systems. Within a pipeline, wettability and film growth will dictate how easily the system

https://doi.org/10.1021/acs.langmuir.1c02136
Langmuir 2021, 37, 12447−12456

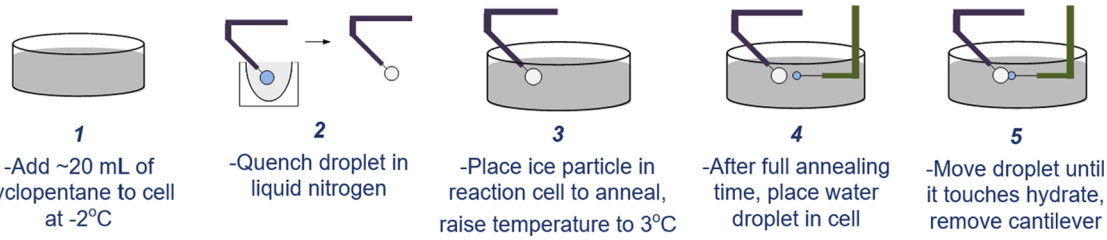

Figure 2. Illustration of basic steps followed to create *in situ* cyclopentane hydrates and perform contact angle measurements.

may agglomerate due to capillary water bridging (affected by wettability) and sintering (affected by film growth) that eventually lead to viscosification, agglomeration, and pipeline plugging (Figure 1B). Studies on methane hydrates by Freer et al.[34] have shown that hydrate growth is proportional to the degree of subcooling within the temperature range of 1.0−4.0 °C and pressure range of 3.55−9.06 MPa. The reported hydrate growth rates are typically in the range of 40−80 μm/s. The same pattern has been observed for CO_2 hydrates by Uchida et al.,[35] who reported lateral growth rates in the range from 6 to 15 mm/s at pressures and subcoolings in the range of 15−25 MPa and 1−5 °C, respectively. This indicates that the film growth will be faster at higher subcoolings, which is also expected for the CyC5 system studied herein. A linear film growth rate of CyC5 at moderate subcoolings has been reported by Morrissy et al.[36] of 2.2 ± 0.2 μm/s. The term "linear" is used to indicate that the film growth that occurs over the three-dimensional water droplet is measured on a microscope image of the film, where only two dimensions are accurately captured. Essentially, the film growth length is considered as the linear distance between the point where the droplet initially met the hydrate surface and the leading edge of the new hydrate film. The same definition of linear film growth rate is used in this work. Hydrate film thickness has also been studied at the water/hydrocarbon interface;[37,38] although important, this parameter will not be the focus of this paper.

To complement and reconcile existing and somewhat contradicting literature observations, two interconnected interfacial studies have been designed here to investigate both contact angle and linear film growth rate of a water droplet on a pure CyC5 hydrate surface surrounded by bulk liquid CyC5. Previous hydrate film growth studies have focused on growth in porous sediments[39] or at the water/fluid hydrocarbon interface.[37] Previous hydrate contact angle studies[24,26,28] were focused on wettability behavior and not film growth. There is limited information on these two parameters for CyC5 hydrates as a function of annealing time and subcooling in the literature. CyC5 hydrates are chosen here because they are often used as a baseline sII hydrate analogue for studying gas hydrates, particularly in the presence of other natural or commercial additives.[40−42] Therefore, understanding the wettability and film growth (especially their coupled behavior) as a function of physical properties will have an immense impact for flow assurance applications and perhaps also other applications such as gas transport,[43] sequestration,[44] and other areas of sustainable chemistry[45] using hydrates. The first part of this work systematically examines the relationship of the contact angle/film growth with varying annealing time (i.e., conversion time), and the second part examines the relationship between contact angle/film growth with varying amounts of subcooling (i.e., hydrate surface roughness).

EXPERIMENTAL SECTION

Materials and Apparatus. CyC5 (OmniSolve CX2414-1, 99% purity) was used in this study as it forms a stable sII hydrate at moderate conditions (atmospheric pressure, 0−7.7°) and acts as an excellent analogue to natural gas hydrates formed within petroleum flowlines. CyC5 hydrates require an ice seed to induce hydrate formation in a timely manner. Because spontaneous nucleation from a liquid water droplet can take more than 24 h,[46] ice seeds are widely used for similar hydrate experiments in the literature.[26,47] This ensures that droplets added to the system will not convert to hydrate while in bulk CyC5, thus allowing testing of *in situ* contact angles and film growth rates on the hydrate surface. DI water was used to form both the hydrate particles/surfaces and the water droplets tested.

The contact angle apparatus consists of an Olympus IX71 microscope equipped with an Olympus XM10 camera and a manual, 3-axis Narishige micromanipulator. The reaction cell is a cylindrical, stainless steel cell with a 12 mm diameter glass viewing window on the bottom and an open-top (ID = 46 mm, height = 23 mm, wall thickness = 2 mm). The volume of the reaction cell is approximately 30 cm^3. This cell is placed in a cooling jacket attached to a glycol chiller, allowing for temperature control.

Technique. Approximately 20−25 mL of chilled (~5 °C) CyC5 is added to the reaction cell maintained at −2 °C. To create the hydrate particle, a water droplet is added to the end of the glass cantilever and quenched in liquid nitrogen to create an ice particle. This is quickly transferred to the reaction cell, prefilled with CyC5. Next, the cell temperature is increased to 3 °C for the remainder of the experiment (above the ice melting point) to induce hydrate formation. The hydrate particle is then left to anneal (i.e., convert to hydrate) undisturbed for a designated amount of time. After the annealing time, a water droplet is added to the end of a thin glass fiber (~30 μm in diameter) cantilever, which is placed in the manual manipulator. The droplet is then placed on the surface of the hydrate and, the glass fiber cantilever is removed upon contact. This process is illustrated in Figure 2. The placement of the droplet and subsequent film growth is recorded with OLYMPUS Stream 1.7 software. ImageJ v1.52v software is used to extract experimental data from the images and movies. It should be noted that the development of this technique is based on that described by Brown et al. concerning the micromechanical force (MMF) apparatus.[26]

RESULTS AND DISCUSSION

Effect of Annealing Time. The first set of experiments focused on the behavior of both the contact angle and the linear film growth rate as a function of annealing time. Annealing time can be thought of as the total conversion time or the time between hydrate formation and measurements, where the system is left undisturbed while the ice particle converts to hydrate. For this set of experiments, the annealing time is considered to start once the system reaches the designated temperature (i.e., 3 °C). Four annealing times were tested: 15 min, 30 min, 1 h, and 2 h. As shown in Figure 3, the contact angle increases as the annealing time increases. After the annealing time has elapsed, a water droplet is deposited on the hydrate, and the contact angle is measured. Each data point represents an average measurement taken as soon as the water

https://doi.org/10.1021/acs.langmuir.1c02136
Langmuir 2021, 37, 12447−12456

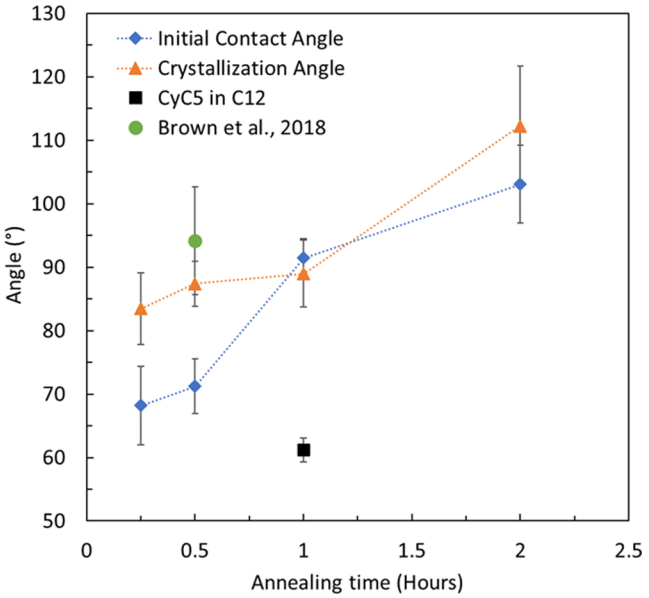

Figure 3. Contact angle and crystallization angle measurements for cyclopentane hydrates in bulk cyclopentane at 3 °C and atmospheric pressure at varying annealing times. The green circle is the value published by Brown et al.[26] The black square represents a measurement on a cyclopentane hydrate in an *n*-dodecane/cyclopentane mixture at the same thermodynamic conditions (final angle with no film growth = 17°; also see Figure S1 for more details). Each measurement represents at least eight different water droplets and at least four different hydrate particles. The error bars represent the standard deviation of these measurements. The dotted lines are guides for the eye.

droplet was deposited on the hydrate to reduce the likelihood of hydrate film growth within the water droplet. Each data point is an average value of at least eight different water droplets deposited on at least four different hydrate particles. The error bars represent the standard deviation of these measurements. As previously stated, the hydrate particle forms initially as a porous structure filled with water, and over time, these pores are filled by further hydrate conversion. With equivalent driving force, a longer annealing time should yield hydrate surfaces that are less porous and "drier"[48] with fewer pathways for water to enter the hydrate and/or spreading over the hydrate surface. This interpretation is consistent with the increase in the contact angle (i.e., decrease in the wettability) observed in our experiments at longer annealing times (Figure 3).

A new and potentially important phenomenon was observed where, upon film growth, the angle between the hydrate surface and the now solid hydrate film surrounding the water droplet increases and stabilizes over time compared to the initial contact angle reported in Figure 3. The final angle will be further referred to as the crystallization angle. This behavior was more apparent at the shorter annealing times (15 and 30 min), where the crystallization angle approached values close to 90° (Figure 3). At an annealing time of 2 h, the crystallization angle reached the larger value of 112°. The crystallization angle measurements shown are an average of angle measurements taken approximately every 30 s from the time the hydrate film was clearly visible to the time film growth had completed. The crystallization angle usually became stable after about 30−60 s of film growth from the beginning of the contact angle measurement. To attempt to minimize the impact of film growth on the contact angle, a contact angle measurement was performed on a fully formed CyC5 hydrate in an *n*-dodecane (C12)/CyC5 mixture (56 vol % C12, a nonhydrate former, diluting the hydrate former; see Figure 3). Here, no film growth was observed, and the contact angle was lower (61.2 ± 1.9°), indicating the role that film growth is having in addition to surface porosity. The droplet was also pulled into the hydrate surface, similar to the procedure described by Thomas et al.[28] but over a longer period of time. Visualizations of this process are shown in Figure S1. The error bars in these data points represent one standard deviation of the measurements conducted for each water droplet. A visual comparison of the contact angles and crystallization angles for each annealing time can be seen in Figure 4. It is noted that the droplets in Figure 4 are not all of the same size due to size control limitations with the experimental system. However, all drops are on the same order of magnitude and are considered similar for these comparisons. The induced morphology changes on the surface of the droplet due to film growth are discussed later on.

The linear film growth rate measured at the same magnitude of subcooling across the water droplet (Figure 5) did not appear to be a function of annealing time, consistently yielding a value of 2.0 ± 0.2 μm/s, where the error represents the standard deviation of measurements across 32 separate water droplets and 19 separate hydrate particles at varying annealing times. This suggests that annealing time does not play a role in

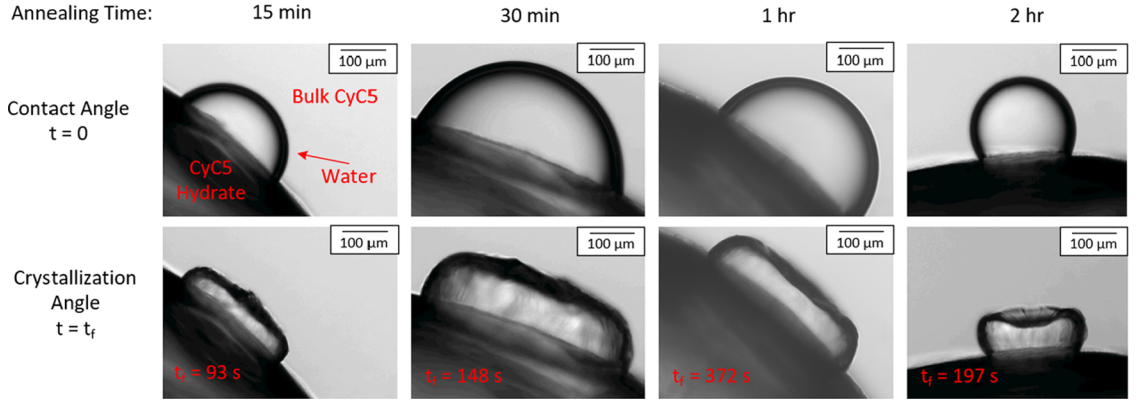

Figure 4. Water droplets placed onto cyclopentane hydrate surfaces in bulk cyclopentane at 3 °C and atmospheric pressure, both after the initial contact ($t = 0$), where it is assumed no film growth has occurred and after film growth has completed ($t = t_f$) for each of the tested annealing times.

https://doi.org/10.1021/acs.langmuir.1c02136
Langmuir 2021, 37, 12447−12456

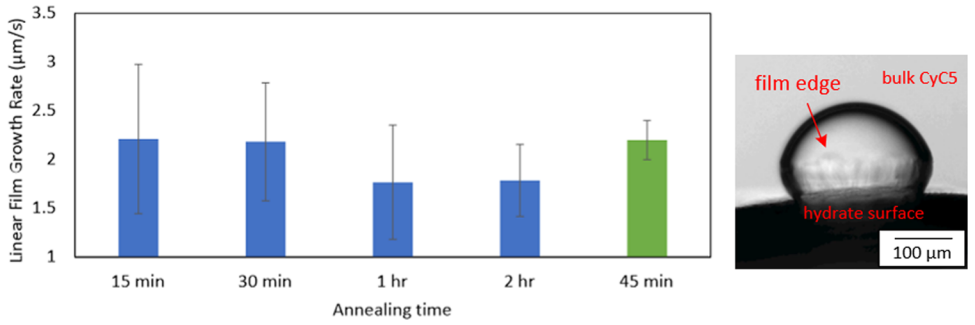

Figure 5. Left: Measured film growth rate of a water droplet on a cyclopentane hydrate surface at 3 °C and atmospheric pressure at varying annealing (conversion) times (blue) compared to a similar system from Morrissy et al. (green).[36] Each measurement represents at least eight different water droplets and at least four different hydrate particles. The error bars represent the standard deviation of these measurements. Right: Hydrate film growing on the water droplet in contact with a cyclopentane hydrate surface.

film growth kinetics. Rather the driving force (i.e., the magnitude of subcooling) plays a larger role in film growth rate, as shown in the following section. This linear growth rate value closely matches the result for a similar system published by Morrissy et al., who reported a film growth rate of 2.2 ± 0.2 μm/s for a system of the same subcooling.[36]

Effect of Subcooling. The second set of experiments focused on both contact angle and the linear film growth rate as a function of the subcooling. Here, the subcooling (ΔT_{sub}) is defined as the temperature difference between the equilibrium temperature (T_{eq} = 7.7 °C) and the system temperature (T_{system}; i.e., $\Delta T_{sub} = T_{eq} - T_{system}$). The subcoolings tested were 1.7 °C (T_{system} = 6 °C), 2.5 °C (T_{system} = 5.2 °C), 4.7 °C (T_{system} = 3 °C), and 6.2 °C (T_{system} = 1.5 °C). As shown in Figure 6, the contact angle initially increases with increasing subcooling (i.e., decreasing T_{system}). This is thought to occur because the hydrate surface is rougher/drier at higher subcoolings, making it more difficult for the water droplet to spread before film growth begins. Evidence of roughness is discussed in the next section. The crystallization angle also changes with subcooling, yielding values consistently larger than the contact angle. The contact and crystallization angle measurements shown are an average of measurements on 4−6 different hydrate particles, with crystallization angle measurements taken at 30 s up to 3-min intervals (depending on subcooling) from the time the film was clearly visible to the time film growth had completed (Figure 6). Our observations suggest that the crystallization angle value did not change with time after the initial (~30 s) film growth occurs. The errors bars represent one standard deviation of the measurements.

The subcooling had a strong effect on the linear film growth rate, which appears to follow a power law trend as a function of the subcooling temperature (Figure 7). Similar trends have been reported for film growth of CO_2 hydrates by Uchida et al.[35] and for methane hydrates by Taylor et al.[37] A direct relationship between film growth rate and subcooling was

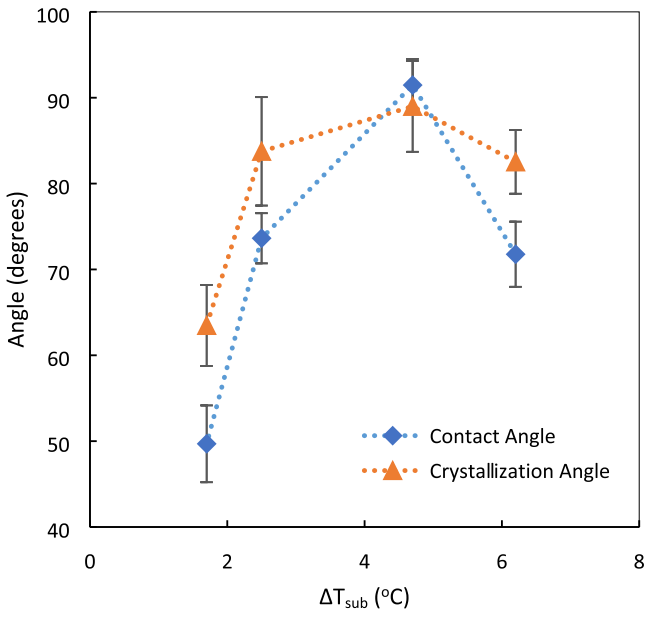

Figure 6. Contact angle as a function of subcooling for a water droplet deposited on a cyclopentane hydrate in bulk cyclopentane at atmospheric pressure with 1 h of annealing time. Each data point represents at least five different water droplets and at least four different hydrate particles. The error bars represent the standard deviation of these measurements. The dotted lines are guides to the eye.

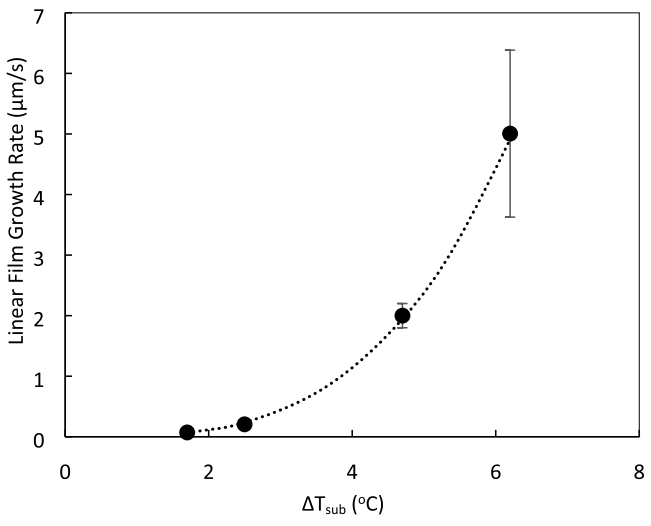

Figure 7. Linear film growth rate as a function of subcooling for a water droplet deposited on a cyclopentane hydrate in bulk cyclopentane at atmospheric pressure after 1 h of annealing time. Each data point represents at least five different water droplets and at least four different hydrate particles. The error bars represent the standard deviation of these measurements. The dotted line is the fitted power function.

https://doi.org/10.1021/acs.langmuir.1c02136
Langmuir 2021, 37, 12447−12456

expected, as a higher subcooling (i.e., a lower system temperature) establishes a larger driving force for hydrate formation, thus resulting in faster film growth across the surface of the water droplet. It should also be noted that the range of CyC5 hydrate film growth rates observed in liquid CyC5 in this work is about 2 orders of magnitude slower than that reported for hydrates in a gas phase.[37] It is expected that a variety of parameters, including the presence of surfactants and impurities, as well as the solubility of the guest molecules in water, can affect the growth rates.

Generally, upon contact of the water droplet to the hydrate surface, higher subcooling resulted in less spreading than low subcooling, except for ΔT_{sub} = 6.2 °C. Spreading at low subcoolings stopped within 1−2 s after the placement of the droplet on the hydrate. At each subcooling, capillary suction, where the droplet was drawn into the hydrate, occurred upon film growth, resulting in a change from a convex liquid droplet to a concave film-covered droplet (see images in Figure 4). The induced morphology changes are discussed in detail in the next section. The results for contact angle and crystallization angle at ΔT_{sub} = 4.7 °C are within the error of each other, but they are consistent with the crystallization angles obtained for ΔT_{sub} of 2.5 and 6.2 °C. This may indicate a threshold of subcooling, where heat transfer effects and roughness are no longer competing, and the roughness is not allowing for much spreading of the water droplet. The results obtained at the subcooling of 6.2 °C were somewhat different, even though the crystallization angle was larger than the contact angle, as observed for the other systems. Even though we expect that high subcooling yields rough hydrate surfaces, a high hydrate film growth rate, and would reduce the spread of the water droplet upon contact resulting in a large contact angle, it might be that the fast water-hydrate conversion rate on a rough substrate favors some leakage of water from the core of the hydrate, rendering the hydrate somewhat "wet". Servio and Englezos[31] suggested that high driving forces (i.e., high subcooling) result in faster and more random crystal growth with higher evidence of heat-limited growth, perhaps leading to some local surface melting (due to the exothermic hydrate crystallization process). A combination of these yields a wetter hydrate surface, favoring more spreading and a smaller contact angle.

The error bars for ΔT_{sub} = 6.2 °C shown in Figure 7 are much larger than those for the other data points. It should be noted that the film growth is initially faster and becomes slower over time due to heat transfer limitations.[37] This effect was larger at higher subcoolings as hydrate formation had a higher driving force. The lower subcoolings saw a decrease in linear film growth rate over time but to a smaller degree, due to the corresponding smaller driving forces (this is shown by the smaller error bars; data point covers error bars for ΔT_{sub} = 1.7, 2.5 °C). An example of the film growth behavior over time for each subcooling can be seen in Figure 8, where the linear growth rate is plotted as a function of observation time after the droplet is deposited on the hydrate surface. Here, it can be noted that the film growth rate slows down over time, which is attributed to the onset of heat transfer limitations from exothermic hydrate film formation seen in other film growth experiments.[37]

Morphology Changes. As shown in Figure 4, the hydrate linear film growth causes the smooth surface of the water droplet to become rough and dimpled. A dimpling effect on the surface of CyC5 hydrates was also observed when an

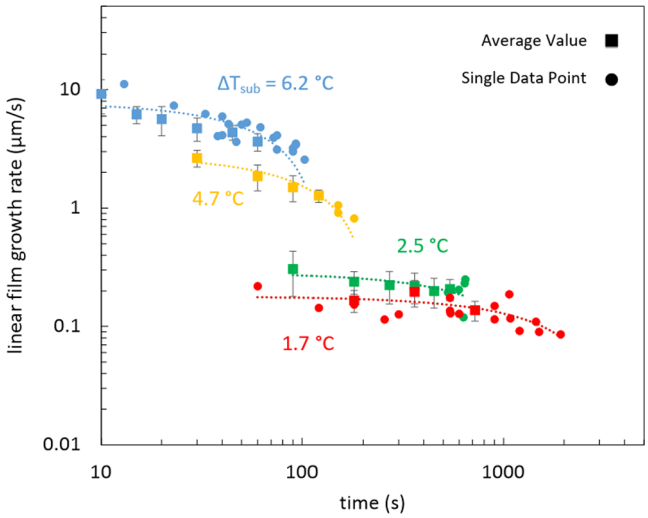

Figure 8. Instantaneous linear film growth rate of cyclopentane hydrate at atmospheric pressure and varying subcoolings with 1 h of annealing time on a log−log plot. The dotted lines represent a linear fit line for each subcooling.

isolated water droplet was seeded with hydrate.[37] The film growth also induces a change in the contact angle, yielding the crystallization angle as discussed in Figure 6. The change in droplet shape from convex to concave is thought to be due to the water being drawn into the hydrate via capillary action, as shown by Davies et al.[27]

The change from the contact angle to the crystallization angle can be thought of conceptually as a four-step process, illustrated in Figure 9:

(1) Deposition and spreading of the water droplet
   a Initial spreading upon deposition of the water droplet onto the hydrate surface: As shown by Thomas et al.,[28] the droplet seeks to spread over the hydrate surface and can do so if the surface is very smooth. However, surface abnormalities may slow the spreading. During this slowed spread, if the subcooling is sufficiently high, hydrate film growth at the three-phase contact point begins. Our results suggest that this growth can occur over the first few seconds after deposition.
   b Water continues spreading but it is slightly hindered by film growth: The hydrate film is very small, thin, and malleable, and not strong enough to stop water spreading, as it is more flexible than rigid. The spreading over the initial hydrate film pushes the film outward, causing an increase of the crystallization angle compared to the contact angle. It is hypothesized that the increase from the initial contact angle to the crystallization angle is a manifestation of the water droplet attempting to minimize its free energy by continuing to spread over the hydrate surface because it can initially overcome the mechanical force of the growing film on the liquid water experienced at the three-phase line. Eventually, the mechanical force outweighs free energy minimization, and the angle stabilizes.
(2) Film growth continues and blocks droplet spread: Once the film reaches a certain height, it is strong enough to stop water spreading. Now, water will diffuse into the

https://doi.org/10.1021/acs.langmuir.1c02136
Langmuir 2021, 37, 12447−12456

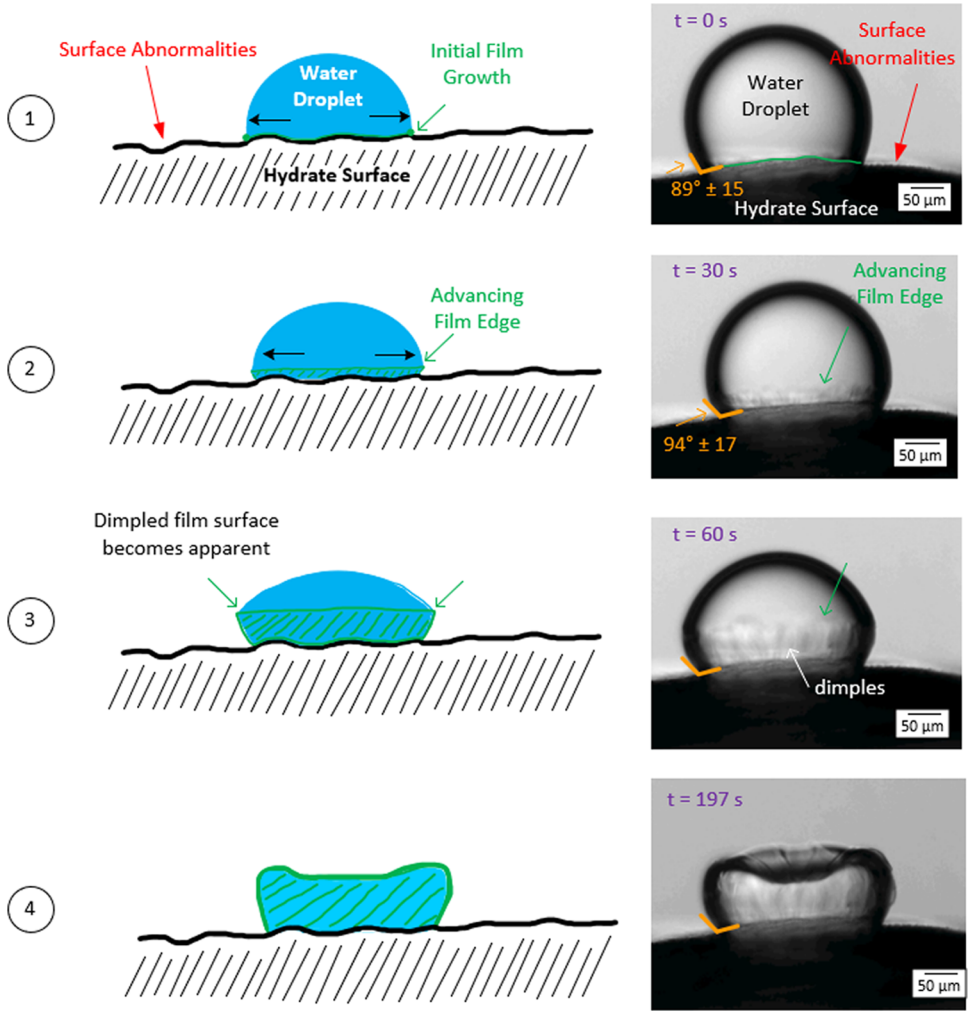

Figure 9. Conceptual picture of the morphology changes brought on by hydrate film growth compared to real images (right). (1) Droplet contacts the hydrate surface (bottom). (2) Film growth begins, and the droplet can no longer spread on the hydrate. (3) Film growth continues as water is drawn into the hydrate (bottom surface), and the shape of the droplet begins to change. (4) Film growth completes and causes the shape to change from convex to concave.

hydrate surface via the pores on the substrate as the hydrate film continues to grow up the water droplet. At this point, the crystallization angle becomes stable because the hydrate film is rigid.

(3) Continuing film growth partially covers the water droplet surface, and the shape of the droplet begins to change: More water is drawn into the hydrate surface, and the droplet begins changing from a convex shape to a concave shape as the hydrate film growth continues.

(4) Film growth is completed: A solid hydrate film covers the entire water droplet surface, whose shape stabilizes.

Depending on the magnitude of the subcooling, this entire process (steps 1−4) may occur between approximately 1 min for high subcoolings to over 30 min for low subcoolings.

Coupling of Wettability and Hydrate Film Growth with Physical Properties. Based on the results outlined above, as well as on those published by Thomas et al.[28] and Brown et al.,[26] we suggest that the discrepancies in the published values of the contact angle of water on CyC5 can be attributed to the state of the hydrate surface. The hydrate surfaces used by Thomas et al.[28] are packed into a cuvette using a scalpel to reduce any deformities or pores in the surface, and the resulting materials are visibly smoother (in terms of the magnitude of peaks/troughs or other surface abnormalities) than those used in this paper and those used by Brown et al.[26] Thomas et al.'s[28] hydrate surface can likely be considered fully annealed as it is left to form over the course of approximately 24 h. On the contrary, the surfaces used in this work are subjected to the morphology of the ice particles used as a precursor to seed the hydrates, as well as any dendrite-like growth induced by high magnitudes of subcooling, as shown in Figure 10. The water droplets used by Thomas et al.[28] are also not temperature-controlled, which causes a local loss of thermodynamic equilibrium, where the droplet contacts the hydrate, essentially reversing the effect of their long annealing time. Based on the data presented showing that annealing time and subcooling affect the contact angle and film growth on the droplet, these two factors play significant and coupled roles in the different observed contact angles. Understanding how these different environmental and interfacial factors affect wetting and film growth is very important, especially since hydrates in flow assurance will likely never be perfectly smooth, and the time-dependent interactions/growth behavior of water-hydrate interfaces are key to the agglomeration and plugging risk assessments, as probed for example in the OLGA process simulator.[49]

https://doi.org/10.1021/acs.langmuir.1c02136
Langmuir 2021, 37, 12447−12456

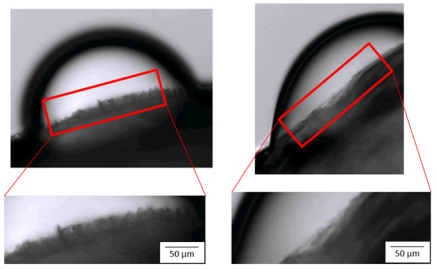

Figure 10. Changes in hydrate surface roughness due to differences in subcooling. Higher subcoolings induce faster hydrate growth, resulting in dendrite-like growth, attributed to heat transfer effects. Lower subcooling allows slower hydrate growth that can expel heat more easily, resulting in a smoother surface.

CONCLUSIONS

An experimental program was conducted to quantify the coupled effect of annealing time and subcooling on the wettability and hydrate film growth on a CyC5 hydrate in pure CyC5. Longer annealing times resulted in larger contact and crystallization angles but did not affect the linear hydrate film growth rate at fixed subcooling. As the contact angle and crystallization angle differ, advancing and receding contact angle studies to further understand these differences would be interesting in the future, but a new technique would need to be developed to overcome the obstacle of film growth at the three-phase line. The linear hydrate film growth rate was found to increase as the degree of subcooling increases because of a larger driving force. However, the instantaneous film growth rate decreased over time, attributed to heat transfer limitations. The results presented here suggest that wettability and hydrate growth rate are coupled, with higher subcooling yielding a general decrease in the wettability due to increased surface roughness and an increased linear film growth rate. At the highest subcooling considered here, the fast hydrate growth promotes competition between different phenomena, including those due to a rough surface and surface heating due to excess heat generated by exothermic crystallization, allowing for the existence of surface water that enhances the wettability. The results suggest that surface abnormalities (i.e., porosity and roughness) and the onset of film growth are leading to the large differences in observed contact angles. A new phenomenon was also observed, according to which the angle created by the new hydrate film grown between the hydrate surface and the bulk liquid (which was defined as the crystallization angle) is consistently larger than the initial contact angle observed for the liquid water droplet on the hydrate surface. This was attributed to a combination of phenomena, including pinning of the water droplet by the growing hydrate film coupled with first the spreading, and then diffusion of water into the hydrate particle. This interpretation is supported by experiments conducted for a system in which crystal growth was prevented—in these systems, contact angles smaller than those discussed in the rest of this paper were obtained. Because the results are obtained on hydrate particles that retain many of the imperfections expected for hydrates in practical applications, the quantification of the phenomena described here is likely to play major role in the prevention of risks due to the agglomeration of hydrates in pipelines and other equipment used by the energy sector. As CyC5 hydrates are also used to test the performance of other pipeline components and additives, it is important to understand the baseline behavior of pure CyC5 hydrate systems created *in situ*. This allows for a full understanding of the relative changes when production fluids or other surface-active components are added to the CyC5 system when studying the wetting and interfacial behavior.

ASSOCIATED CONTENT

Supporting Information

The Supporting Information is available free of charge at https://pubs.acs.org/doi/10.1021/acs.langmuir.1c02136.

Additional contact angle images from experiments performed on cyclopentane hydrate in a cyclopentane/*n*-dodecane mixture (PDF)

AUTHOR INFORMATION

Corresponding Author

Carolyn A. Koh − *Center for Hydrate Research, Department of Chemical and Biological Engineering, Colorado School of Mines, Golden, Colorado 80401, United States;* orcid.org/0000-0003-3452-4032; Email: ckoh@mines.edu

Authors

Hannah M. Stoner − *Center for Hydrate Research, Department of Chemical and Biological Engineering, Colorado School of Mines, Golden, Colorado 80401, United States*

Anh Phan − *Department of Chemical Engineering, University College London, London WC1E 7JE, U.K.;* orcid.org/0000-0003-2428-6990

Alberto Striolo − *Department of Chemical Engineering, University College London, London WC1E 7JE, U.K.;* Present Address: School of Chemical, Biological and Materials Engineering University of Oklahoma Norman, OK 73019, United States; orcid.org/0000-0001-6542-8065

Complete contact information is available at: https://pubs.acs.org/10.1021/acs.langmuir.1c02136

Notes

The authors declare no competing financial interest.

ACKNOWLEDGMENTS

The authors would like to thank the NSF CBET Award #201520 (H.M.S. and C.A.K.) and EPSRC #EP/T004282/1 (A.P. and A.S.) for funding. Thanks also to the Center for Hydrate Research for the facilities used for this study.

ABBREVIATIONS

sIstructure I; sIIstructure II; sHstructure H; THFtetrahydrofuran; CyC5cyclopentane; C12*n*-dodecane; MMFmicromechanical force

REFERENCES

(1) Makogon, Y. Features of Natural Gas Fields Exploitation in Permafrost Zone. *Gazov. Prom-sti.* **1966**, *9*, 1−17.

(2) Hammerschmidt, E. G. Formation of Gas Hydrates in Natural Gas Transmission Lines. *Ind. Eng. Chem.* **1934**, *26*, 851−855.

(3) Gudmundsson, J. S.; Mork, M.; Graff, O. F. In *Hydrate Non-Pipeline Technology*, 4th International Conference on Gas Hydrates, Yokohama, 2002; pp 19−23.

(4) Xu, H.; Khan, M. N.; Peters, C. J.; Sloan, E. D.; Koh, C. A. Hydrate-Based Desalination Using Cyclopentane Hydrates at Atmospheric Pressure. *J. Chem. Eng. Data* **2018**, *63*, 1081−1087.
(5) Khan, M. N.; Peters, C. J.; Koh, C. A. Desalination Using Gas Hydrates: The Role of Crystal Nucleation, Growth and Separation. *Desalination* **2019**, *468*, No. 114049.
(6) Xu, C.; Chen, Z.; Cai, J.; Li, X. Study on Pilot-Scale CO 2 Separation from Flue Gas by the Hydrate Method. *Energy Fuels* **2014**, *28*, 1242−1248.
(7) Yang, M.; Zhou, H.; Wang, P.; Li, N.; Song, Y. Hydrate-Based CO2 Capture from Flue Gas in Constant Pressure Process with the Presence of THF. *Energy Procedia* **2017**, *142*, 3939−3943.
(8) Sloan, E. D.; Koh, C. A. *Clathrate Hydrates of Natural Gases*, 3rd ed.; CRC Press: Boca Raton, FL, 2008.
(9) Yang, S. O.; Kleehammer, D. M.; Huo, Z.; Sloan, E. D.; Miller, K. T. Temperature Dependence of Particle-Particle Adherence Forces in Ice and Clathrate Hydrates. *J. Colloid Interface Sci.* **2004**, *277*, 335−341.
(10) Strobel, T. A.; Taylor, C. J.; Hester, K. C.; Dec, S. F.; Koh, C. A.; Miller, K. T.; Sloan, E. D. Molecular Hydrogen Storage in Binary THF-H2 Clathrate Hydrates. *J. Phys. Chem. B* **2006**, *110*, 17121−17125.
(11) Delahaye, A.; Fournaison, L.; Marinhas, S.; Chatti, I.; Petitet, J. P.; Dalmazzone, D.; Fürst, W. Effect of THF on Equilibrium Pressure and Dissociation Enthalpy of CO 2 Hydrates Applied to Secondary Refrigeration. *Ind. Eng. Chem. Res.* **2006**, *45*, 391−397.
(12) Taylor, C. J.; Dieker, L. E.; Miller, K. T.; Koh, C. A.; Sloan, E. D. Micromechanical Adhesion Force Measurements between Tetrahydrofuran Hydrate Particles. *J. Colloid Interface Sci.* **2007**, *306*, 255−261.
(13) Dieker, L. E.; Taylor, C. J.; Koh, C. A.; Sloan, E. D. In *Micromechanical Adhesion Force Measurements between Cyclopentane Hydrate Particles*, 6th International Conference on Gas Hydrates, Vancouver, 2008.
(14) Dieker, L. E. Cyclopentane Hydrate Interparticle Adhesion Force Measurements. M.S. Thesis, Colorado School of Mines: Golden, CO, 2009.
(15) Culberson, O. L.; McKetta, J. J. Phase Equilibria in Hydrocarbon-Water Systems III - The Solubility of Methane in Water at Pressures to 10,000 PSIA. *J. Pet. Technol.* **1951**, *3*, 223−226.
(16) Kobayashi, R.; Katz, D. Vapor-Liquid Equilibria For Binary Hydrocarbon-Water Systems. *Ind. Eng. Chem.* **1953**, *45*, 440−446.
(17) Østergaard, K. K.; Tohidi, B.; Danesh, A.; Burgass, R. W.; Todd, A. C. Equilibrium Data and Thermodynamic Modelling of Isopentane and 2,2,-Dimethylpentane Hydrates. *Fluid Phase Equilib.* **2000**, *169*, 101−115.
(18) Barrio-Zhang, H.; Ruiz-Gutiérrez, É.; Armstrong, S.; Mchale, G.; Wells, G. G.; Ledesma-aguilar, R. Contact-Angle Hysteresis and Contact-Line Friction on Slippery Liquid-like Surfaces. *Langmuir* **2020**, *36*, 15094−15101.
(19) Bormashenko, E. Y. 2 - Wetting of Surfaces: The Contact Angle. In *Physics of Wetting: Phenomena and Applications of Fluids on Surfaces*; de Gruyter: Berlin, 2017; pp 20−39.
(20) Stoner, H. M.; Koh, C. A. Perspective on the Role of Particle Size Measurements in Gas Hydrate Agglomeration Predictions. *Fuel* **2021**, *304*, No. 121385.
(21) Palermo, T.; Fidel-Dufour, A.; Maurel, P.; Peytavy, J. L.; Hurtevent, C. In *Model of Hydrates Agglomeration - Application to Hydrates Formation in an Acidic Crude Oil*, 12th International Conference on Multiphase Production Technology; OnePetro, 2005; pp 525−540.
(22) Asserson, R. B.; Hoffmann, A. C.; Høiland, S.; Asvik, K. M. Interfacial Tension Measurement of Freon Hydrates by Droplet Deposition and Contact Angle Measurements. *J. Pet. Sci. Eng.* **2009**, *68*, 209−217.
(23) Song, J. H.; Couzis, A.; Lee, J. W. Investigation of Macroscopic Interfacial Dynamics between Clathrate Hydrates and Surfactant Solutions. *Langmuir* **2010**, *26*, 18119−18124.
(24) Aman, Z. M.; Leith, W. J.; Grasso, G. A.; Sloan, E. D.; Sum, A. K.; Koh, C. A. Adhesion Force between Cyclopentane Hydrate and Mineral Surfaces. *Langmuir* **2013**, *29*, 15551−15557.
(25) Hu, S.; Koh, C. A. Interfacial Properties and Mechanisms Dominating Gas Hydrate Cohesion and Adhesion in Liquid and Vapor Hydrocarbon Phases. *Langmuir* **2017**, *33*, 11299−11309.
(26) Brown, E. P.; Hu, S.; Wells, J.; Wang, X.; Koh, C. A. Direct Measurements of Contact Angles on Cyclopentane Hydrates. *Energy Fuels* **2018**, *32*, 6619−6626.
(27) Davies, S. R.; Sloan, E. D.; Sum, A. K.; Koh, C. A. In Situ Studies of the Mass Transfer Mechanism across a Methane Hydrate Film Using High-Resolution Confocal Raman Spectroscopy. *J. Phys. Chem. C* **2010**, *114*, 1173−1180.
(28) Thomas, F.; Dalmazzone, D.; Morris, J. F. Contact Angle Measurements on Cyclopentane Hydrates. *Chem. Eng. Sci.* **2021**, *229*, No. 116022.
(29) Zylyftari, G.; Ahuja, A.; Morris, J. F. Nucleation of Cyclopentane Hydrate by Ice Studied by Morphology and Rheology. *Chem. Eng. Sci.* **2014**, *116*, 497−507.
(30) Wenzel, R. N. Resistance of Solid Surfaces to Wetting by Water. *Ind. Eng. Chem.* **1936**, *28*, 988−994.
(31) Servio, P.; Englezos, P. Morphology of Methane and Carbon Dioxide Hydrates Formed from Water Droplets. *AIChE J.* **2003**, *49*, 269−276.
(32) Lehmkühler, F.; Paulus, M.; Sternemann, C.; Lietz, D.; Venturini, F.; Gutt, C.; Tolan, M. The Carbon Dioxide-Water Interface at Condtions of Gas Hydrate Formation. *J. Am. Chem. Soc.* **2009**, *131*, 585−589.
(33) Li, S. L.; Sun, C. Y.; Liu, B.; Li, Z. Y.; Chen, G. J.; Sum, A. K. New Observations and Insights into the Morphology and Growth Kinetics of Hydrate Films. *Sci. Rep.* **2014**, *4*, No. 4129.
(34) Freer, E. M.; Sami Selim, M.; Dendy Sloan, E. Methane Hydrate Film Growth Kinetics. *Fluid Phase Equilib.* **2001**, *185*, 65−75.
(35) Uchida, T.; Ikeda, I. Y.; Takeya, S.; Ebinuma, T.; Nagao, J.; Narita, H. CO2 Hydrate Film Formation at the Boundary between CO2 and Water: Effects of Temperature, Pressure and Additives on the Formation Rate. *J. Cryst. Growth* **2002**, *237*−*239*, 383−387.
(36) Morrissy, S. A.; McKenzie, A. J.; Graham, B. F.; Johns, M. L.; May, E. F.; Aman, Z. M. Reduction of Clathrate Hydrate Film Growth Rate by Naturally Occurring Surface Active Components. *Energy Fuels* **2017**, *31*, 5798−5805.
(37) Taylor, C. J.; Miller, K. T.; Koh, C. A.; Sloan, E. D. Macroscopic Investigation of Hydrate Film Growth at the Hydrocarbon/Water Interface. *Chem. Eng. Sci.* **2007**, *62*, 6524−6533.
(38) Brown, E. P.; Koh, C. A. Micromechanical Measurements of the Effect of Surfactants on Cyclopentane Hydrate Shell Properties. *Phys. Chem. Chem. Phys.* **2016**, *18*, 594−600.
(39) Almenningen, S.; Lysyy, M.; Ersland, G. Quantification of CH4Hydrate Film Growth Rates in Micromodel Pores. *Cryst. Growth Des.* **2021**, *21*, 4090−4099.
(40) Aspenes, G.; Dieker, L. E.; Aman, Z. M.; Høiland, S.; Sum, A. K.; Koh, C. A.; Sloan, E. D. Adhesion Force between Cyclopentane Hydrates and Solid Surface Materials. *J. Colloid Interface Sci.* **2010**, *343*, 529−536.
(41) Chen, Z.; Liu, B.; Manica, R.; Liu, Q.; Xu, Z. Interaction between the Cyclopentane Hydrate Particle and Water Droplet in Hydrocarbon Oil. *Langmuir* **2020**, *36*, 2063−2070.
(42) Bui, T.; Phan, A.; Monteiro, D.; Lan, Q.; Ceglio, M.; Acosta, E.; Krishnamurthy, P.; Striolo, A. Evidence of Structure-Performance Relation for Surfactants Used as Antiagglomerants for Hydrate Management. *Langmuir* **2017**, *33*, 2263−2274.
(43) Kezirian, M. T.; Phoenix, S. L. Natural Gas Hydrate as a Storage Mechanism for Safe, Sustainable and Economical Production from Offshore Petroleum Reserves. *Energies* **2017**, *10*, No. 828.
(44) Lee, Y.; Choi, W.; Shin, K.; Seo, Y. CH4-CO2 Replacement Occurring in SII Natural Gas Hydrates for CH4 Recovery and CO2 Sequestration. *Energy Convers. Manage.* **2017**, *150*, 356−364.
(45) Hassanpouryouzband, A.; Joonaki, E.; Vasheghani Farahani, M.; Takeya, S.; Ruppel, C.; Yang, J.; English, N. J.; Schicks, J. M.;

Edlmann, K.; Mehrabian, H.; et al. Gas Hydrates in Sustainable Chemistry. *Chem. Soc. Rev.* **2020**, *49*, 5225−5309.
(46) Larsen, R.; Lund, A.; Andersson, V.; Hjarbo, K. W. In *Conversion of Water to Hydrate Particles*, Proceedings - SPE Annual Technical Conference and Exhibition; OnePetro, 2001; pp 1905−1909.
(47) Aman, Z. M.; Brown, E. P.; Sloan, E. D.; Sum, A. K.; Koh, C. A. Interfacial Mechanisms Governing Cyclopentane Clathrate Hydrate Adhesion/Cohesion. *Phys. Chem. Chem. Phys.* **2011**, *13*, 19796−19806.
(48) Høiland, S.; Askvik, K. M.; Fotland, P.; Alagic, E.; Barth, T.; Fadnes, F. Wettability of Freon Hydrates in Crude Oil/Brine Emulsions. *J. Colloid Interface Sci.* **2005**, *287*, 217−225.
(49) Wang, Y.; Subramanian, S.; Estanga, D.; Majid, A. A. A.; Hu, S.; Salmin, D. C.; Koh, C. A.; Zerpa, L. E. Changing the Hydrate Management Guidelines: From Benchtop Experiments to CSMHyK Field Simulations. *Energy Fuels* **2020**, *34*, 13523−13535.

https://doi.org/10.1021/acs.langmuir.1c02136
Langmuir 2021, 37, 12447−12456